Multi-Material 3D Printing of Functional Ceramic Devices

Subjects: Engineering, Manufacturing | Chemistry, Applied

Contributor: Hui Chen , Liang Guo , Wenbo Zhu , Chunlai Li

As an emerging technology, multi-material 3D printing offers increased complexity and greater freedom in the design of functional ceramic devices because of its unique ability to directly construct arbitrary 3D parts that incorporate multiple material constituents without an intricate process or expensive tools.

multi-material | 3D printing | functional ceramic devices | capacitors | multilayer substrates | microstrip antennas

1. Introduction

Compared with structural ceramics, functional ceramic devices are characterized by their detection, transformation, coupling, transmission, processing, and storage of information (i.e., electrical, magnetic, optical, acoustic, thermal, force, and biological [1]), and they have been used in numerous fields (i.e., aviation, automobile, integrated circuit, communication, medical, and energy) [2]. Most functional ceramic devices, such as multilayer ceramic capacitors, multilayer ceramic substrates, filters, chip antennas, power dividers, and duplexers, can be fabricated by a high-temperature cofired ceramic (HTCC) process or low-temperature cofired ceramic (LTCC) process [3][4][5][6][7][8]. These processes require multiple steps: (1) material preparation for ceramic tapes and functional pastes, (2) punching of the green tapes for via formation, (3) filling and metalizing for vertical conductors and horizon circuitries formation, (4) stacking and laminating for 3D ceramic green body formation that can be maintained as an array or cut into individual products, (5) cofiring, and (6) post processing including nickel plating, brazing, and gold plating (**Figure 1**) [9]. As a result, the metal pastes (e.g., silver, gold, tungsten, and molybdenum) and resistor pastes can be cofired with the ceramic body to fabricate multilayer ceramic components. With the continuous development of electronic science and technology, the HTCC and LTCC processes are poorly suited to the rapid prototyping and low-cost manufacturing of miniaturized, thin, refined, and highly integrated functional ceramic devices.

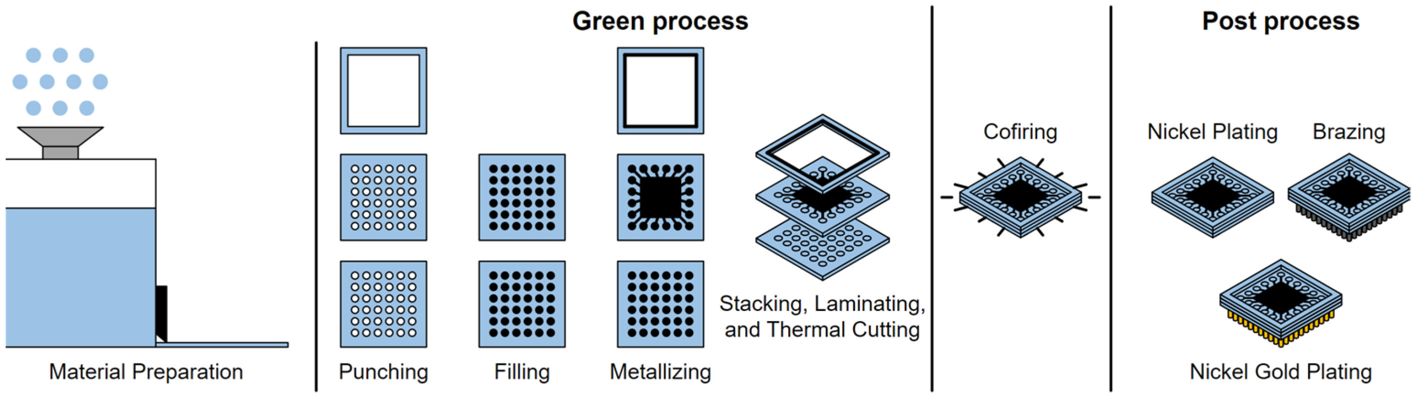

Figure 1. Cofired ceramic process.

Three-dimensional printing is a breakthrough manufacturing method that can build 3D objects layer-by-layer from digital models and has developed rapidly since the 1980s. Three-dimensional printing is commonly known as additive manufacturing (AM), and the ASTM/ISO standard for AM classifies the different technologies into seven subcategories: material extrusion, material jetting, binder jetting, vat photopolymerization, powder bed fusion, direct energy deposition, and sheet object lamination [10]. According to this classification, HTCC and LTCC based on green tape lamination can also be considered an AM process, though different from 3D printing; therefore, to distinguish this concept, the researchers use the term “3D printing” rather than “AM”.

In recent years, 3D printing has become a research focus in fine ceramic manufacturing, and it can be used to construct most structural ceramics [11][12][13][14]. However, functional ceramic devices with a composite structure comprising two or more materials usually contain strip lines, microstrip lines, and vias; as a result, in addition to enhancing the spatial resolution and printing speed, several problems in terms of the raw materials, printing strategies, and sintering process still need to be solved. Multi-material 3D printing of functional ceramic devices is in early development and has great research motivation and application potential [15][16][17][18][19].

2. Multi-Material 3D Printing Methods

2.1. Material Jetting (MJ)

MJ derives from conventional 2D ink jetting extensively used in graphic fields (e.g., office documents, digital photos, labels, tiles, and clothing) [20]. In MJ, droplets of the feedstock material are selectively deposited and solidified in successive layers [21]. Several MJ techniques are recognized by the mechanism of droplet generation, in which the most widely used are inkjet printing (IJP), aerosol jet printing (AJP), and electrohydrodynamic inkjet printing (EHDP). Over the past few years, these MJ techniques have attracted interest in the on-demand fabrication of highly customizable electronics because of their abilities to precisely and smartly deliver high-resolution patterns with a diversified structure (<1 µm) from design files in a non-contact manner. Multi-material 3D printing of supercapacitors [22], filters [23], tapered optical waveguides [24], solar cells [25], microsensors [26], flexible circuits [27], and high-density redistribution layers (RDLs) of silicon interposers [28] has been easily implemented by following the same approach of conventional 2D ink jetting by sequential deposition of functional inks via an MJ system equipped with multiple jetting heads. **Table 1** lists several recently developed functional inks whose printing methods, applications, sintering or curing techniques, and electrical properties are summarized.

Table 1. Summary of recently developed functional inks.

Types of Functional Inks	Printing Methods	Applications	Electrical Properties
Metal nanoparticles (MNPs) inks	Sliver MNPs inks; IJP [29], EHD [27]	Wearable electronics [27] [29]	0.08–4.74 Ω sq^{-1} after 1 h of thermal sintering at 150 °C [29]; 0.4 Ω sq^{-1} after 30 min of thermal sintering at 250 °C [27]
	Gold MNPs inks; IJP [30], AJP [31]	Non-enzymatic electrochemical sensors [30]; micro-hotplates [31]	0.06 Ω cm^{-1} after 30 min thermal sintering at 100 °C [30]; 8.7 ± 2.5 µΩ cm after 1 h of thermal sintering at 120 °C followed by 250 °C for 4 h [31]
	Copper MNPs inks; IJP [32], EHD [33]	Conductive patterns and tracks [32]; micro-electronic devices [33]	6.18 Ω sq^{-1} after applying 5454 J energy [32]; 9.20 µΩ cm after 1 h of thermal sintering at 230 °C in inert atmosphere [33]
	Zinc MNPs inks; IJP [34], AJP [35]	Flexible electronics [34]; bioresorbable electronics [35]	~10^2 S cm^{-1} [34]; 22.32 S cm^{-1} was achieved after 2 ms of sintering by 1 flash with energy of 25.88 J/cm^2, and the final conductivity of 34.72 S cm^{-1} was achieved by an optimum laser power [35]
Conductive polymer inks	PEDOT: PSS inks; IJP [36], AJP [37]	Organic solar cells [36]; µ-needle electrode arrays [37]	0.02 S cm^{-1} after 20 min of thermal annealing at 120 °C (120 nm thick) [36]; 0.323 ± 0.075 S cm^{-1} [37]
	BBL: PEI inks; Spray-coating [38]	Organic electrochemical transistors and bioelectronics [38]	8 S cm^{-1} after 2 h of thermal annealing at 140 °C inside a nitrogen-filled glovebox [38]

Types of Functional Inks	Printing Methods	Applications	Electrical Properties
Ceramic nanoparticle (CNP) inks	Al_2O_3 CNPs inks; IJP [39]	Thin film radio-frequency capacitors [39]	The dielectric constant of the printed alumina layer (~120 nm thick with ~0.5 nm RMS surface roughness after the thermal annealing at 400 °C) was 6.2 [39]
	$BaTiO_3$ CNPs inks; IJP [40], AJP [41]	Piezoelectric generators [40]; interdigitated capacitors [41]	The piezoelectric generator had an open-circuit voltage of ~7 V, a current density of 0.21 $\mu A \cdot cm^{-2}$, and a power density of 0.42 $\mu W \cdot cm^{-2}$ [40]; the dielectric constant was 7 [41]
	3Y-TZP CNPs inks; IJP [42][43]	Dielectric films for microelectronic devices [42][43]	/
	ZrO_2 CNPs inks; IJP [44], EHD [45]	Dielectric layers for flexible electronics [44]; resistive switches [45]	The ZrO_2 dielectric film (dielectric constant of 10) afforded a leakage current density of 5.4×10^{-6} A/cm^2 at 1 MV/cm [44]. The printed resistive switch showed stable bipolar memristive switching behavior around ± 3 V [45]
	TiO_2 CNPs inks; IJP [46][47]	Mesoporous TiO_2 electron transport layers for perovskite solar cells [46]; dielectric layers [47]	The perovskite solar cell had a power conversion efficiency of 18.29% [46]; the current-voltage characteristics of conducting oxide-TiO_2-Ag devices showed diode behavior [47]
	$Ba_{0.6}Sr_{0.4}TiO_3$ CNPs inks; IJP [48]	Dielectric layers for capacitors [48]	The relative dielectric constant was 28 ± 1.7, and the dielectric loss was 0.043 ± 0.006 (at 10 kHz) [48]

Types of Functional Inks	Printing Methods	Applications	Electrical Properties
Dielectric polymer inks	$Ca_2Nb_3O_{10}$ CNPs inks; AJP [49]	Thin-film transistors [49]	The films deposited by $Ca_2Nb_3O_{10}$ ink with a mass fraction of 82 wt% showed a dielectric constant of 8.5 and a dielectric loss of 0.058 (at 1 MHz) [49]
	Glass silicate CNPs inks; IJP [50]	Multilayer hybrid circuits [50]	/
	Polyimide (PI) inks; IJP [51]	Capacitors for microelectronic devices [51]	The printed capacitor with 25 ± 0.2 µm thick PI layer showed a capacitance value of 103 pF [51]
	Poly 4-vinylphenol (PVP) inks; IJP [52]	Flexible capacitors for wearable electronics [52]	The printed capacitor with 4.5 µm thick PVP layer showed a capacitance value of 163 pF [52]
	Polyvinyl alcohol (PVA) inks; EHD [53]	Gate insulators in organic field-effect transistors [53]	The organic field-effect transistors with PVA-based gate insulators show stable operation with low gate leakage currents [53]

2.2. Direct Ink Writing (DIW)

DIW originated from robocasting technology, which was initially established by Cesarani et al. at Sandia National Laboratories in 1997. As an extrusion-based versatile 3D printing method, DIW provides a powerful route for fabricating complex 3D structures with high aspect ratio walls or spanning elements at the meso- and microscale from polymers (conductive or insulating) [54][55], ceramic particles [56][57], metal particles [58], graphene nanosheets [59], carbon nanotubes (CNTs) [60], and composites [61]. During printing, the ink (also called a suspension or paste) with shear thinning behavior is pneumatically or screw-extruded through a motion-controlled nozzle (typical diameter 100–500 μm, **Figure 2**a) and then deposited on the platform to form precise patterns. To steadily stack multiple layers and guarantee fidelity and structural integrity, the extruded ink must fully solidify instantaneously, which is assisted by an optional post-curing process (solvent evaporation, gelation, solvent-driven reactions,

s;
nso, L.;
viron.
g. 2010,
26, 44–50.

4. Thelemann, T.; Bartnitzek, T.; Suphan, K.-H.; Apel, S. Advancing packaging solutions using 3D capabilities of ceramic multilayers. In Proceedings of the 2015 European Microelectronics Packaging Conference (EMPC), Friedrichshafen, Germany, 14–16 September 2015; pp. 1–6.
5. Oshima, S.; Wada, K.; Murata, R.; Shimakata, Y. Multilayer Dual-Band Bandpass Filter in Low-Temperature Co-Fired Ceramic Substrate for Ultra-Wideband Applications. IEEE Trans. Microw. Theory Tech. 2010, 58, 614–623.
6. Liu, Z.; Wang, P.; Zeng, Z. Enhancement of the Gain for Microstrip Antennas Using Negative Permeability Metamaterial on Low Temperature Co-Fired Ceramic (LTCC) Substrate. IEEE Antennas Wirel. Propag. Lett. 2013, 12, 429–432.
7. Chen, H.; Che, W.; Wang, X.; Feng, W. Size-Reduced Planar and Nonplanar SIW Gysel Power Divider Based on Low Temperature Co-fired Ceramic Technology. IEEE Microw. Wirel. Compon.

thermal treatment, and photoradiation) to allow for crosslinking [62]. **Figure 2**b shows a modified UV-assisted DIW setup [63].

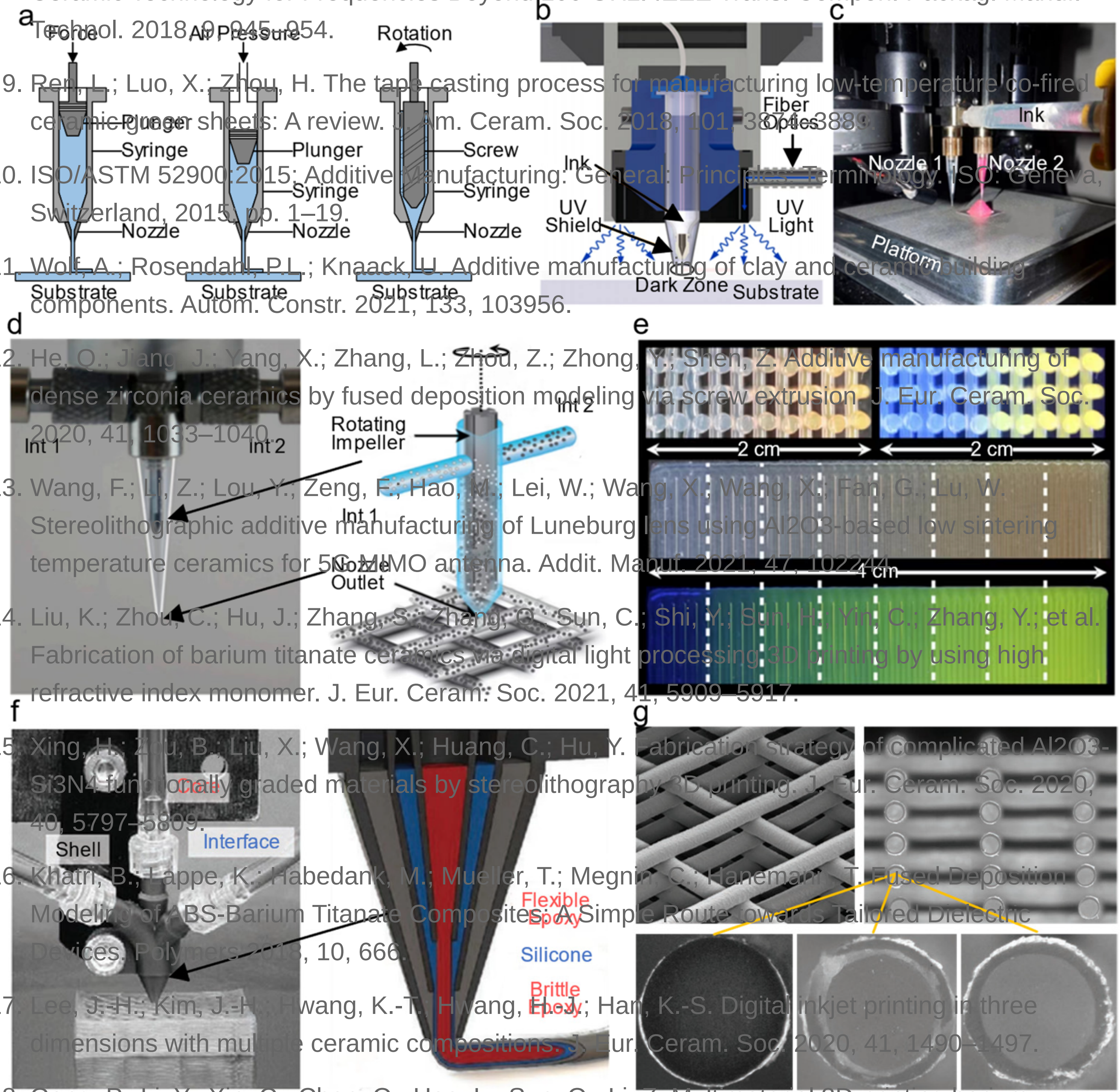

Figure 2. (**a**) Schematics of plunger-based extrusion, pneumatic-based extrusion, and screw-based extrusion of DIW. (**b**) Cross sectional view of the UV-assisted DIW process [63]. (**c**) Multi-material 3D printing with a dual nozzle DIW system [64]. (**d**) Optical image and schematic illustration of the impeller-based active mixer for multi-material DIW and (**e**) cross sectional images of the printed 3D rectangular lattice structure showing continuous change in the fluorescent pigment concentration [65]. (**f**) Optical image and schematic illustration of the multicore-shell nozzle

Lett. 2017, 27, 1065–1067.

8. Bhutani, A.; Gottel, B.; Lipp, A.; Zwick, T. Packaging Solution Based on Low-Temperature Cofired Ceramic Technology for Frequencies Beyond 100 GHz. IEEE Trans. Compon. Packag. Manuf. Technol. 2018, 9, 945–954.
9. Ren, L.; Luo, X.; Zhou, H. The tape casting process for manufacturing low-temperature co-fired ceramic green sheets: A review. J. Am. Ceram. Soc. 2018, 101, 3874–3889.
10. ISO/ASTM 52900:2015; Additive Manufacturing: General Principles Terminology. ISO: Geneva, Switzerland, 2015; pp. 1–19.
11. Wolf, A.; Rosendahl, P.L.; Knaack, U. Additive manufacturing of clay and ceramic building components. Autom. Constr. 2021, 133, 103956.
12. He, Q.; Jiang, J.; Yang, X.; Zhang, L.; Zhou, Z.; Zhong, Y.; Shen, Z. Additive manufacturing of dense zirconia ceramics by fused deposition modeling via screw extrusion. J. Eur. Ceram. Soc. 2020, 41, 1033–1040.
13. Wang, F.; Li, Z.; Lou, Y.; Zeng, F.; Hao, M.; Lei, W.; Wang, X.; Wang, X.; Fan, G.; Lu, W. Stereolithographic additive manufacturing of Luneburg lens using Al2O3-based low sintering temperature ceramics for 5G MIMO antenna. Addit. Manuf. 2021, 47, 102244.
14. Liu, K.; Zhou, C.; Hu, J.; Zhang, S.; Zhang, Q.; Sun, C.; Shi, Y.; Sun, H.; Yin, C.; Zhang, Y.; et al. Fabrication of barium titanate ceramics via digital light processing 3D printing by using high refractive index monomer. J. Eur. Ceram. Soc. 2021, 41, 5909–5917.
15. Xing, H.; Zou, B.; Liu, X.; Wang, X.; Huang, C.; Hu, Y. Fabrication strategy of complicated Al2O3-Si3N4 functionally graded materials by stereolithography 3D printing. J. Eur. Ceram. Soc. 2020, 40, 5797–5809.
16. Khatri, B.; Lappe, K.; Habedank, M.; Mueller, T.; Megnin, C.; Hanemann, T. Fused Deposition Modeling of ABS-Barium Titanate Composites: A Simple Route towards Tailored Dielectric Devices. Polymers 2018, 10, 666.
17. Lee, J.-H.; Kim, J.-H.; Hwang, K.-T.; Hwang, H.-J.; Han, K.-S. Digital inkjet printing in three dimensions with multiple ceramic compositions. J. Eur. Ceram. Soc. 2020, 41, 1490–1497.
18. Gong, P.; Li, Y.; Xin, C.; Chen, Q.; Hao, L.; Sun, Q.; Li, Z. Multimaterial 3D-printing barium titanate/carbonyl iron composites with bilayer-gradient honeycomb structure for adjustable broadband microwave absorption. Ceram. Int. 2021, 48, 9873–9881.
19. Smay, J.E.; Nadkarni, S.S.; Xu, J. Direct Writing of Dielectric Ceramics and Base Metal Electrodes. Int. J. Appl. Ceram. Technol. 2007, 4, 47–52.
20. Castrejon-Pita, J.R.; Baxter, W.; Morgan, J.; Temple, S.; Martin, G.; Hutchings, I.M. Future, opportunities and challenges of inkjet technologies. At. Sprays 2013, 23, 541–565.

connected to the core, interface, and shell ink syringes for multi-material DIW, and (g) cross-sectional images of the printed rectangular lattice structure [66].

Various material and process parameters, for instance, the rheological properties of the ink (e.g., viscosity and surface tension), the geometric features of the nozzle, extrusion pressure, standoff distance, printing speed, strip spacing, and curing technique, significantly dictate the quality (e.g., dimensional error, surface roughness, layer flatness, and interfacial strength) of the printed 3D parts [67][68]. Several essential capabilities of qualified inks for DIW include the ability to flow easily through the nozzle when subjected to a shear force, sufficiently high yield strength after extrusion, and self-supportability. The feature resolution is positively correlated with the size of the nozzle. Although smaller nozzles provide higher feature resolution, they sacrifice build efficiency, and a greater extrusion pressure is required to enable smooth flow of the viscoelastic ink at the risk of nozzle damage. Notably, DIW with a nozzle diameter ranging from 0.5 μm to 5 μm has been used to create structures with feature sizes ranging from 100 nm to 10 μm [69].

There are three different strategies enabling multi-material 3D printing with DIW (multi-material DIW) according to the nozzle design and ink extrusion mode. The first is that multiple inks stored separately in their individual syringes are extruded through multiple nozzles to construct multi-material structures layer-by-layer (**Figure 2**c) [64][70]. This strategy is the most commonly used and involves switching between multiple nozzles for sequential printing, which requires accurate coordination of each nozzle and careful flow control of viscoelastic inks, especially when the printed inks have different rheological properties [71]. The second uses a single nozzle with the capability of switching between inks or in situ mixing of multiple inks via a mixing impeller driven by rotary motor during the printing process while simultaneously controlling the printed geometry (**Figure 2**d–e) [65][72][73]. This strategy makes it possible to fabricate functionally graded patterns with tunable properties (e.g., strength, coefficient of thermal expansion, and permittivity). The third strategy uses a multicore-shell nozzle with several specific inputs connected to corresponding syringes, which enables the coextrusion of multiple inks to form a core-shell filament (**Figure 2**f–g) [66][74].

Recently, multi-material DIW has been increasingly adopted to manufacture functionally graded structures (e.g., triboelectric nanogenerators [75], sensors [76], supercapacitors [77][78], photodetectors [79], batteries [70], circuit board [80], and scaffolds [81]) because of its unique ability to separately or simultaneously extrude different functional inks. For example, Sears et al. [81] used a multi-material DIW printer to fabricate a scaffold with a poly(ε-caprolactone) (PCL) or poly(lactic acid) (PLA) shell and a propylene fumarate dimethacrylate (PFDMA) hierarchical architecture. The addition of the PCL or PLA shell resulted in a significant increase in the compressive modulus and yield strength. Natural bone tissue comprises hierarchical porous structures that support cell growth, provide space for nutrient transport, and withstand different types of ambient loads [82]. Critical size or non-union bone defects can be treated by surgically implanting biocompatible bone graft substitutes [83]. However, there are many problems in the long-term use of biocompatible bone graft substitutes, such as displacement, allergic reaction, and the need for secondary surgery [84]. Another permanent solution is to facilitate bone tissue regeneration via a scaffold. Multi-material DIW has garnered considerable attention because of its potential in constructing the heterogeneous and anisotropic structure that can enable scaffolds to mimic the properties of natural bone tissue [58][85]. In addition,

21. Dilag, J.; Chen, T.; Li, S.; Bateman, S.A. Design and direct additive manufacturing of three-dimensional surface micro-structures using material jetting technologies. Addit. Manuf. 2019, 27, 167–174.
22. Choi, K.-H.; Yoo, J.; Lee, C.K.; Lee, S.-Y. All-inkjet-printed, solid-state flexible supercapacitors on paper. Energy Environ. Sci. 2016, 9, 2812–2821.
23. Craton, M.T.; Sorocki, J.; Piekarz, I.; Gruszczynski, S.; Wincza, K.; Papapolymerou, J. Realization of fully 3D printed W-band bandpass filters using aerosol jet printing technology. In Proceedings of the 2018 48th European Microwave Conference (EuMC), Madrid, Spain, 25–27 September 2018; pp. 1013–1016.
24. Theiler, P.M.; Lütolf, F.; Ferrini, R. Non-contact printing of optical waveguides using capillary bridges. Opt. Express 2018, 26, 11934–11939.
25. Eggenhuisen, T.M.; Galagan, Y.; Biezemans, A.F.K.V.; Slaats, T.M.W.L.; Voorthuijzen, W.P.; Kommeren, S.; Shanmugam, S.; Teunissen, J.P.; Hadipour, A.; Verhees, W.J.H.; et al. High efficiency, fully inkjet printed organic solar cells with freedom of design. J. Mater. Chem. A 2015, 3, 7255–7262.
26. Qin, H.; Dong, J.; Lee, Y.-S. Fabrication and electrical characterization of multi-layer capacitive touch sensors on flexible substrates by additive e-jet printing. J. Manuf. Process. 2017, 28, 479–485.
27. Khan, A.; Rahman, K.; Ali, S.; Khan, S.; Wang, B.; Bermak, A. Fabrication of circuits by multi-nozzle electrohydrodynamic inkjet printing for soft wearable electronics. J. Mater. Res. 2021, 36, 3568–3578.
28. Laurila, M.-M.; Khorramdel, B.; Mäntysalo, M. Combination of E-Jet and Inkjet Printing for Additive Fabrication of Multilayer High-Density RDL of Silicon Interposer. IEEE Trans. Electron Devices 2017, 64, 1217–1224.
29. Karim, N.; Afroj, S.; Tan, S.; Novoselov, K.S.; Yeates, S.G. All Inkjet-Printed Graphene-Silver Composite Ink on Textiles for Highly Conductive Wearable Electronics Applications. Sci. Rep. 2019, 9, 8035.
30. Kant, T.; Shrivas, K.; Tapadia, K.; Devi, R.; Ganesan, V.; Deb, M.K. Inkjet-printed paper-based electrochemical sensor with gold nano-ink for detection of glucose in blood serum. New J. Chem. 2021, 45, 8297–8305.
31. Khan, S.; Nguyen, T.; Lubej, M.; Thiery, L.; Vairac, P.; Briand, D. Low-power printed micro-hotplates through aerosol jetting of gold on thin polyimide membranes. Microelectron. Eng. 2018, 194, 71–78.
32. Lim, S.; Joyce, M.; Fleming, P.D.; Aijazi, A.T.; Atashbar, M. Inkjet Printing and Sintering of Nano-Copper Ink. J. Imaging Sci. Technol. 2013, 57, 50506-1–50506-7.

triply periodic minimal surface (TPMS) scaffolds allow for precise geometric modification; as a result, many physical characteristics (e.g., surface-to-volume ratio, pore size, elastic properties, and fluid behaviors) can be controlled [86].

2.3. Fused Deposition Modeling (FDM)

FDM is one of the most extensively used 3D printing techniques for polymer structures (e.g., polylactic acid, butadiene styrene, polycarbonate, polyamide, polystyrene, and polyethylene [87]) because of its inexpensive apparatus cost and easy implementation. FDM is also known as fused filament fabrication (FFF); in this process, the thermoplastic polymer filament is melted or softened in a liquefier head, and then the polymer is selectively extruded by the action of two counter rotating elements on the platform to build the 3D objects in a layer-on-layer manner. Over the past few years, thermoplastic polymer filaments reinforced by a variety of fillers, such as metals [88][89], ceramics [90][91][92][93], fibers [94][95], and bioactive glass [96], have been developed. With enhanced properties (e.g., mechanical strength, thermal conductivity, permittivity, dielectric loss, and biocompatibility) of these composite filaments, FDM greatly expands its application scope into electronic, automotive, aerospace, biomedical, and sports industries.

The critical parameters of FDM are filament-specific (e.g., thermal, mechanical, and rheological properties and diameter), operation-specific (e.g., temperature, speed, and structure of 3D-printed object), and apparatus-specific (e.g., number of extrusion heads, nozzle diameter, and gear force) [97][98]. Multi-material 3D printing with FDM (multi-material FDM) can be easily implemented using multiple extrusion nozzles, and the method has drawn increasing interest. However, some inherent disadvantages still exist when multi-material FDM is used to construct complex structures, such as low resolution accompanied by poor surface finish, insufficient bonding between adjacent sections, and slow build velocity [71]. Additionally, thermoplastic polymer filaments with high solid content are necessary for the fabrication of metal and ceramic parts because of the low shrinkage after sintering; However, the dramatic increase in stiffness and brittleness adversely affects the production and printing process [99]. Therefore, significant efforts should be devoted to overcoming these challenges.

2.4. Vat Photopolymerization (VP)

In the vat photopolymerization (VP) process, a liquid-state photopolymer material housed in a vat is selectively cured and patterned by light-initiated polymerization [10]. This class of technologies includes stereolithography (SLA), two-photon lithography (2PL) or two-photon polymerization (2PP), digital light processing (DLP), and continuous liquid interface production (CLIP).

As one of the oldest VP technologies established by Hull in 1984, SLA uses a UV laser beam scanning quickly along a controlled path to cure the irradiated photopolymer material within a vat from point to point. After one slice is printed, the build platform moves downward or lifts (depending on if the machine is a top-down or bottom-up structure) with a constant amount equaling exactly one-slice thickness in the z-direction for the next slice printing until the 3D part is finished [100]. Another important laser scanning technology, 2PL, differs from conventional

33. Khan, A.; Rahman, K.; Kim, D.S.; Choi, K.H. Direct printing of copper conductive micro-tracks by multi-nozzle electrohydrodynamic inkjet printing process. J. Mater. Process. Technol. 2011, 212, 700–706.

34. Majee, S.; Karlsson, M.C.F.; Wojcik, P.J.; Sawatdee, A.; Mulla, M.Y.; Alvi, N.U.H.; Dyreklev, P.; Beni, V.; Nilsson, D. Low temperature chemical sintering of inkjet-printed Zn nanoparticles for highly conductive flexible electronic components. npj Flex. Electron. 2021, 5, 32.

35. Mahajan, B.K.; Ludwig, B.; Shou, W.; Yu, X.; Fregene, E.; Xu, H.; Pan, H.; Huang, X. Aerosol printing and photonic sintering of bioresorbable zinc nanoparticle ink for transient electronics manufacturing. Sci. China Inf. Sci. 2018, 61, 060412.

36. Singh, A.; Katiyar, M.; Garg, A. Understanding the formation of PEDOT:PSS films by ink-jet printing for organic solar cell applications. RSC Adv. 2015, 5, 78677–78685.

37. Zips, S.; Grob, L.; Rinklin, P.; Terkan, K.; Adly, N.Y.; Weiß, L.J.K.; Mayer, D.; Wolfrum, B. Fully Printed μ-Needle Electrode Array from Conductive Polymer Ink for Bioelectronic Applications. ACS Appl. Mater. Interfaces 2019, 11, 32778–32786.

38. Yang, C.-Y.; Stoeckel, M.-A.; Ruoko, T.-P.; Wu, H.-Y.; Liu, X.; Kolhe, N.B.; Wu, Z.; Puttisong, Y.; Musumeci, C.; Massetti, M.; et al. A high-conductivity n-type polymeric ink for printed electronics. Nat. Commun. 2021, 12, 2354.

39. McKerricher, G.; Maller, R.; Mohammad, V.; McLachlan, M.A.; Shamim, A. Inkjet-printed thin film radio-frequency capacitors based on sol-gel derived alumina dielectric ink. Ceram. Int. 2017, 43, 9846–9853.

40. Lim, J.; Jung, H.; Baek, C.; Hwang, G.-T.; Ryu, J.; Yoon, D.; Yoo, J.; Park, K.-I.; Kim, J.H. All-inkjet-printed flexible piezoelectric generator made of solvent evaporation assisted BaTiO3 hybrid material. Nano Energy 2017, 41, 337–343.

41. Craton, M.T.; He, Y.; Roch, A.; Chahal, P.; Papapolymerou, J. Additively manufactured interdigitated capacitors using barium titanate nanocomposite inks. In Proceedings of the 2019 49th European Microwave Conference (EuMC), Paris, France, 1–3 October 2019; pp. 488–491.

42. Rahul, S.; Balasubramanian, K.; Venkatesh, S. Optimizing inkjet printing process to fabricate thick ceramic coatings. Ceram. Int. 2017, 43, 4513–4519.

43. Özkol, E.; Wätjen, A.M.; Bermejo, R.; Deluca, M.; Ebert, J.; Danzer, R.; Telle, R. Mechanical characterisation of miniaturised direct inkjet printed 3Y-TZP specimens for microelectronic applications. J. Eur. Ceram. Soc. 2010, 30, 3145–3152.

44. Zhu, Z.; Zhang, J.; Zhou, Z.; Ning, H.; Cai, W.; Wei, J.; Zhou, S.; Yao, R.; Lu, X.; Peng, J. A Simple, Low Cost Ink System for Drop-on-Demand Printing High Performance Metal Oxide Dielectric Film at Low Temperature. ACS Appl. Mater. Interfaces 2019, 11, 5193–5199.

(single-photon) SLA by exploiting the two-photon absorption (2PA) process to induce polymerization of the photopolymer material within the focal region of an ultrafast (femtosecond or picosecond) pulsed laser. Therefore, 2PL can be used to fabricate 3D microstructures with feature resolutions beyond the diffraction limit and free from the staircase effect caused by fluctuations of photopolymer materials [101]. However, 2PL shares the same common time-consuming issue as SLA and requires careful design of the highly transparent feedstock, especially when involving light-scattering additives such as ceramic particles [102].

In contrast to the aforementioned laser scanning technologies, DLP employs a digital light projector rather than a laser as the light source. As a result, a 2D image corresponding to each layer shape can be projected over the surface of the photopolymer material within a vat. DLP considerably improves building efficiency because any design can be printed layer-by-layer instead of individually addressing one voxel. Projection micro stereolithography (PμSL) is a development from DLP using a liquid crystal display, a digital micromirror device, or liquid crystals on the silicon device as a dynamic mask and featuring superior resolution (up to 0.6 μm) [103]. CLIP is another development from DLP enabling continuous growth of a 3D part using an oxygen-permeable and UV-transparent window at the bottom of the photopolymer material vat [104]. Oxygen can travel through the window and mix into the liquid photopolymer material, forming a persistent liquid interface (oxygen dead zone) capable of inhibiting free radical photopolymerization. As a result, the build platform no longer needs to move up and down for each layer [105].

These VP-based 3D printing technologies have shown great potential in sensors, actuators, robots, microfluidic devices, and scaffolds because of their ability to construct 3D parts with high resolution, high accuracy, high throughput, and a good surface finish, which is not the case for MJ, DIW, and FDM [106]. However, most studies simply focus on single-material fabrication, and multi-material 3D printing with VP-based technologies remains challenging and limited because of difficulties in exchanging liquid-state photopolymer materials within a vat. In general, three different strategies have been developed: (1) a hybrid process via the combination with DIW, AJP, or other special techniques, (2) vat switching, and (3) dynamic fluidic control. Among a few recently reported applications, the first strategy may be the most straightforward and widely adopted. Lopes et al. [107] presented a hybrid multi-material 3D printing system that integrated SLA and DIW to fabricate monolithic structures with embedded circuits. SLA was used to build substrate structures, reserving the required receptacles into which electronic components were subsequently inserted, and channels and vertical vias were created, while DIW provided the precisely dispensing conductive material into the channels and vertical vias to realize interconnection (**Figure 3**a). Similarly, Peng et al. [108] presented a hybrid multi-material 3D printing system that integrated DLP and DIW to fabricate active soft robots, circuit-embedding architectures, and strain sensors (**Figure 3**b–d). This strategy requires an effective cleaning tool (e.g., air jet, vacuum, brush, and ultrasonic) to remove the uncured photopolymer material from reserved receptacles, channels, and vertical vias, as any material contamination leads to dimensional inaccuracies. With the second strategy, the simplest approach is to manually or automatically exchange the photopolymer material within a vat [109] or switch between multiple vats containing different photopolymer materials [110][111]; however, the printing process has to be interrupted, significantly increasing its time consumption. To overcome this issue, researchers have proposed multi-material stereolithography without vats that can deliver multiple photopolymer materials on a moving glass plate or silicone sled using aerosol jet

45. Awais, M.N.; Kim, H.C.; Doh, Y.H.; Choi, K.H. ZrO2 flexible printed resistive (memristive) switch through electrohydrodynamic printing process. Thin Solid Films 2013, 536, 308–312.

46. Huckaba, A.J.; Lee, Y.; Xia, R.; Paek, S.; Bassetto, V.C.; Oveisi, E.; Lesch, A.; Kinge, S.; Dyson, P.J.; Girault, H.; et al. Inkjet-Printed Mesoporous TiO2 and Perovskite Layers for High Efficiency Perovskite Solar Cells. Energy Technol. 2018, 7, 317–324.

47. Padrón-Hernández, W.; Ceballos-Chuc, M.C.; Pourjafari, D.; Oskam, G.; Tinoco, J.C.; Martínez-López, A.; Rodríguez-Gattorno, G. Stable inks for inkjet printing of TiO2 thin films. Mater. Sci. Semicond. Process. 2018, 81, 75–81.

48. Mikolajek, M.; Friederich, A.; Kohler, C.; Rosen, M.; Rathjen, A.; Krüger, K.; Binder, J.R. Direct Inkjet Printing of Dielectric Ceramic/Polymer Composite Thick Films. Adv. Eng. Mater. 2015, 17, 1294–1301.

49. Wu, X.; Fei, F.; Chen, Z.; Su, W.; Cui, Z. A new nanocomposite dielectric ink and its application in printed thin-film transistors. Compos. Sci. Technol. 2014, 94, 117–122.

50. Singlard, M.; Aimable, A.; Lejeune, M.; Dossou-Yovo, C.; Poncelet, M.; Noguera, R.; Modes, C. Aqueous suspensions of glass silicate dielectric powders for ink-jet-printing applications. Powder Technol. 2014, 266, 303–311.

51. Zhang, F.; Tuck, C.; Hague, R.; He, Y.; Saleh, E.; Li, Y.; Sturgess, C.; Wildman, R. Inkjet printing of polyimide insulators for the 3D printing of dielectric materials for microelectronic applications. J. Appl. Polym. Sci. 2016, 133, 43361–43371.

52. Yi, L.; Torah, R.; Beeby, S.; Tudor, J. An all-inkjet printed flexible capacitor on a textile using a new poly(4-vinylphenol) dielectric ink for wearable applications. In Proceedings of the Sensors, Taipei, Taiwan, 28–31 October 2012.

53. Jung, C.; Tang, X.; Kwon, H.-J.; Wang, R.; Oh, S.M.; Ye, H.; Jeong, Y.R.; Jeong, Y.J.; Kim, S.H. Electrohydrodynamic-Printed Polyvinyl Alcohol-Based Gate Insulators for Organic Integrated Devices. Adv. Eng. Mater. 2022, 24, 2100900.

54. Holness, F.B.; Price, A.D. Direct ink writing of 3D conductive polyaniline structures and rheological modelling. Smart Mater. Struct. 2017, 27, 015006.

55. Gu, S.; Tian, Y.; Liang, K.; Ji, Y. Chitin nanocrystals assisted 3D printing of polycitrate thermoset bioelastomers. Carbohydr. Polym. 2021, 256, 117549.

56. Wang, P.; Li, J.; Wang, G.; He, L.; Yu, Y.; Xu, B. Multimaterial Additive Manufacturing of LTCC Matrix and Silver Conductors for 3D Ceramic Electronics. Adv. Mater. Technol. 2022, 7, 2101462.

57. Jiang, Q.; Yang, D.; Yuan, H.; Wang, R.; Hao, M.; Ren, W.; Shao, G.; Wang, H.; Cui, J.; Hu, J. Fabrication and properties of Si2N2O-Si3N4 ceramics via direct ink writing and low-temperature sintering. Ceram. Int. 2021, 48, 32–41.

systems [112] or pump-based syringes [113][114][115] (**Figure 3**e). In this distinctive process, a bottom-up projection method is mostly adopted, which greatly reduces the amount of resin to be used because the printed part is immersed in the liquid-state photopolymer material at a limited depth [116]. Notably, in combination with an in situ microfuidic system (**Figure 3**f), Chen et al. [117] achieved 3D microlattices with dissimilar constituent materials (**Figure 3**g), which is attractive for manufacturing various structures with tailorable properties such as a negative Poisson's ratio. Miri et al. [118] demonstrated an in situ microfuidic system with several on/off pneumatic valves for fast switching between different photopolymer materials and accomplished the multi-material stereolithography of heterogeneous hydrogel constructs. With the third strategy, recently, Han et al. [119] developed a multi-material PμSL system using dynamic fluidic control to realize rapid filling and exchange of multiple photopolymer materials within an integrated pressure-tight fluidic cell (**Figure 3**h) that is capable of fabricating highly complex heterogeneous 3D microstructures (**Figure 3**i).

58. Xu, C.; Quinn, B.; Lebel, L.L.; Therriault, D.; L'Espérance, G. Multi-material direct ink writing (DIW) for complex 3D metallic structures with removable supports. ACS Appl. Mater. Interfaces 2019, 11, 8499–8506.

59. Li, Z.; Li, Y.; Shi, B.; Tang, D.; Wang, Y.; Hao, L. Dual gradient direct ink writing of functional geopolymer-based carbonyl-iron/graphene composites for adjustable broadband microwave absorption. Ceram. Int. 2022, 48, 9277–9285.

60. Luo, B.; Wei, Y.; Chen, H.; Zhu, Z.; Fan, P.; Xu, X.; Xie, B. Printing Carbon Nanotube-Embedded Silicone Elastomers via Direct Writing. ACS Appl. Mater. Interfaces 2018, 10, 44796–44802.

61. Cheng, M.; Ramasubramanian, A.; Rasul, G.; Jiang, Y.; Yuan, Y.; Foroozan, T.; Deivanayagam, R.; Saray, M.T.; Rojaee, R.; Song, B.; et al. Direct Ink Writing of Polymer Composite Electrolytes with Enhanced Thermal Conductivities. Adv. Funct. Mater. 2021, 31, 2006683.

62. Lewis, J.A. Direct ink writing of 3D functional materials. Adv. Funct. Mater. 2006, 16, 2193–2204.

63. Tu, R.; Sodano, H.A. Additive manufacturing of high-performance vinyl ester resin via direct ink writing with UV-thermal dual curing. Addit. Manuf. 2021, 46, 102180.

64. Li, L.; Lin, Q.; Tang, M.; Duncan, A.J.; Ke, C. Advanced polymer designs for direct-ink-write 3D printing. Chemistry 2019, 25, 10768–10781.

65. Ober, T.J.; Foresti, D.; Lewis, J.A. Active mixing of complex fluids at the microscale. Proc. Natl. Acad. Sci. USA 2015, 112, 12293–12298.

66. Mueller, J.; Raney, J.R.; Shea, K.; Lewis, J.A. Architected Lattices with High Stiffness and Toughness via Multicore–Shell 3D Printing. Adv. Mater. 2018, 30, e1705001.

67. Ahammed, S.R.; Praveen, A.S. Optimization parameters effects on electrical conductivity of 3D printed circuits fabricated by direct ink writing method using functionalized multiwalled carbon nanotubes and polyvinyl alcohol conductive ink. Int. J. Simul. Multidiscip. Des. Optim. 2021, 12, 7.

68. Udofia, E.N.; Zhou, W. Microextrusion based 3D printing—A review. In Proceedings of the 2018 International Solid Freeform Fabrication Symposium, Austin, TX, USA, 13–15 August 2018.

69. Xu, M.; Lewis, J.A. Phase Behavior and Rheological Properties of Polyamine-Rich Complexes for Direct-Write Assembly. Langmuir 2007, 23, 12752–12759.

70. Sun, K.; Wei, T.-S.; Ahn, B.Y.; Seo, J.Y.; Dillon, S.J.; Lewis, J.A. 3D Printing of Interdigitated Li-Ion Microbattery Architectures. Adv. Mater. 2013, 25, 4539–4543.

71. Han, D.; Lee, H. Recent advances in multi-material additive manufacturing: Methods and applications. Curr. Opin. Chem. Eng. 2020, 28, 158–166.

72. Golobic, A.M.; Durban, M.D.; Fisher, S.E.; Grapes, M.; Ortega, J.M.; Spadaccini, C.M.; Duoss, E.B.; Gash, A.E.; Sullivan, K.T. Active Mixing of Reactive Materials for 3D Printing. Adv. Eng.

Mater. 2019, 21, 1900147.

73. Hassan, I.; Selvaganapathy, P.R. A microfluidic printhead with integrated hybrid mixing by sequential injection for multimaterial 3D printing. Addit. Manuf. 2022, 50, 102559.

74. Pack, R.C.; Romberg, S.K.; Badran, A.A.; Hmeidat, N.S.; Yount, T.; Compton, B.G. Carbon Fiber and Syntactic Foam Hybrid Materials via Core–Shell Material Extrusion Additive Manufacturing. Adv. Mater. Technol. 2020, 5, 2000731.

75. Chen, K.; Zhang, L.; Kuang, X.; Li, V.; Lei, M.; Kang, G.; Wang, Z.L.; Qi, H.J. Dynamic Photomask-Assisted Direct Ink Writing Multimaterial for Multilevel Triboelectric Nanogenerator. Adv. Funct. Mater. 2019, 29, 1903568.

76. Kim, S.; Oh, J.; Jeong, D.; Park, W.; Bae, J. Consistent and Reproducible Direct Ink Writing of Eutectic Gallium–Indium for High-Quality Soft Sensors. Soft Robot. 2018, 5, 601–612.

77. Chen, B.; Jiang, Y.; Tang, X.; Pan, Y.; Hu, S. Fully Packaged Carbon Nanotube Supercapacitors by Direct Ink Writing on Flexible Substrates. ACS Appl. Mater. Interfaces 2017, 9, 28433–28440.

78. Jiang, Y.; Cheng, M.; Shahbazian-Yassar, R.; Pan, Y. Direct Ink Writing of Wearable Thermoresponsive Supercapacitors with rGO/CNT Composite Electrodes. Adv. Mater. Technol. 2019, 4, 1900691.

79. Park, S.H.; Su, R.; Jeong, J.; Guo, S.; Qiu, K.; Joung, D.; Meng, F.; McAlpine, M.C. 3D Printed Polymer Photodetectors. Adv. Mater. 2018, 30, e1803980.

80. Hinton, J.; Mirgkizoudi, M.; Campos-Zatarain, A.; Flynn, D.; Harris, R.; Kay, R. Digitally-driven hybrid manufacture of ceramic thick-film substrates. In Proceedings of the 2018 7th Electronic System-Integration Technology Conference (ESTC), Dresden, Germany, 18–21 September 2018; pp. 1–5.

81. Sears, N.; Dhavalikar, P.; Whitely, M.; Cosgriff-Hernandez, E. Fabrication of biomimetic bone grafts with multi-material 3D printing. Biofabrication 2017, 9, 025020.

82. Basu, B. Natural bone and tooth: Structure and properties. In Biomaterials for Musculoskeletal Regeneration; Springer: Berlin/Heidelberg, Germany, 2017; pp. 45–85.

83. Wang, Q.; Xu, L.; Jin, F.; Zheng, W.; Zhang, X.; Huang, Y.; Qian, Z. Artificial periosteum in bone defect repair—A review. Chin. Chem. Lett. 2017, 28, 1801–1807.

84. Li, X.; Yuan, Y.; Liu, L.; Leung, Y.S.; Chen, Y.; Guo, Y.; Chai, Y.; Chen, Y. 3D printing of hydroxyapatite/tricalcium phosphate scaffold with hierarchical porous structure for bone regeneration. Bio-Design Manuf. 2020, 3, 15–29.

85. Betancourt, N.; Chen, X. Review of extrusion-based multi-material bioprinting processes. Bioprinting 2022, 25, e00189.

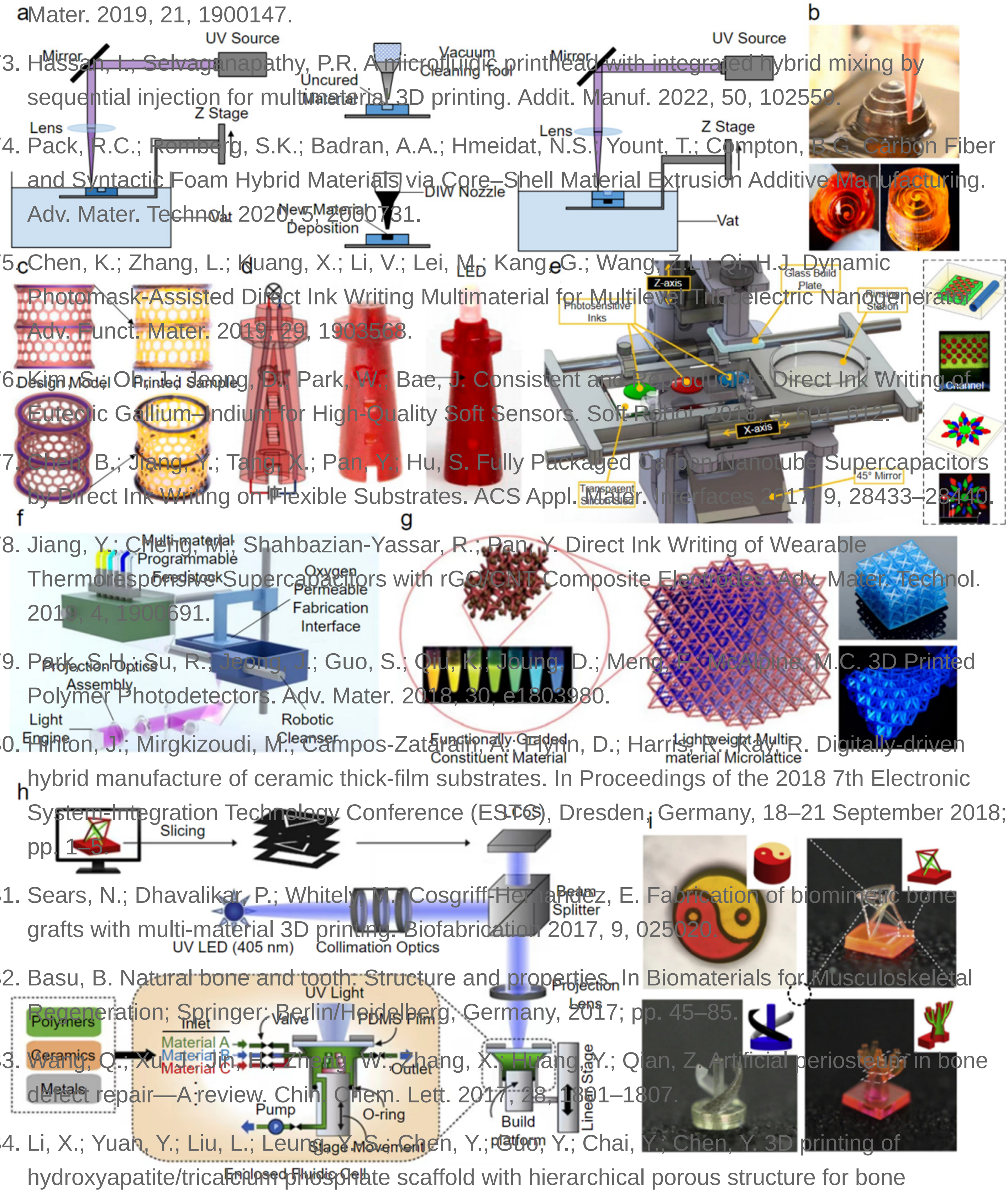

Figure 3. Multi-material 3D printing with VP-based technologies. (**a**) Schematic illustration of the multi-material 3D printing system integrating SLA and DIW. (**b**) Photographs of the printed electronic structure with an embedded 3D helix, (**c**) photographs of the printed cylindrical lattice with three rings embedded, and (**d**) photographs of the

printed light tower [108]. (e) Schematic illustration of the multi-material stereolithography without vats [115]. (f) Schematic illustration of the multi-material stereolithography using an in situ microfluid system, and (g) photographs of the printed 3D microlattice with dissimilar constituent materials [117]. (h) Schematic illustration of the multi-material PuSL system using dynamic fluidic control to rapidly fill and exchange multiple photopolymer materials, and (i) photographs of the printed micro 3D structures [119].

3. Applications of Multi-Material 3D Printing in Functional Ceramic Devices

In most cases, functional ceramic devices with multiple material constituents have tiny structural features such as strip lines, microstrip lines, and vias. These structural features present a challenge for multi-material 3D printing processes because micro-defects will degrade the electrical and mechanical properties. In addition, the materials (ceramics, polymers, and metals) and their compatibility with 3D printing techniques must be further investigated. **Table 2** lists several composition examples of multi-material 3D printing in functional ceramic devices.

Table 2. Several composition examples of multi-material 3D printing in functional ceramic devices.

Compositions	Multi-Material 3D Printing Techniques	Applications	Properties	Ref.
Dielectric material (ink): $Ca_2NaNb_4O_{13}$ + Isopropanol + 2-butyl alcohol Electrode material (ink): Ag	IJP	Capacitors	The capacitor showed a capacitance density of ≈210 pF/mm^2	[120]
Dielectric material (ink): $Ba_{0.6}Sr_{0.4}TiO_3$-ZnO-B_2O_3 + Butyl diglycol + isopropyl alcohol + ethyl cellulose Electrode material (ink): Ag	IJP	Varactors	The varactors showed a tunability between 14.4% and 16.4% under a tuning field of 5 V/μm	[121]
Dielectric material (ink): $MgTiO_3$ Electrode material (ink): Ag	IJP	Capacitors	/	[122]

86. Poltue, T.; Karuna, C.; Khrueaduangkham, S.; Seehanam, S.; Promoppatum, P. Design exploration of 3D-printed triply periodic minimal surface scaffolds for bone implants. Int. J. Mech. Sci. 2021, 211, 106762.

87. Boparai, K.S.; Singh, R.; Singh, H. Development of rapid tooling using fused deposition modeling: A review. Rapid Prototyp. J. 2016, 22, 281–299.

88. Ryder, M.A.; Lados, D.A.; Iannacchione, G.S.; Peterson, A.M. Fabrication and properties of novel polymer-metal composites using fused deposition modeling. Compos. Sci. Technol. 2018, 158, 43–50.

89. Hwang, S.; Reyes, E.I.; Moon, K.-S.; Rumpf, R.C.; Kim, N.S. Thermo-mechanical Characterization of Metal/Polymer Composite Filaments and Printing Parameter Study for Fused Deposition Modeling in the 3D Printing Process. J. Electron. Mater. 2014, 44, 771–777.

90. Castles, F.; Isakov, D.; Lui, A.; Lei, Q.; Dancer, C.; Wang, Y.; Janurudin, J.; Speller, S.; Grovenor, C.; Grant, P.S. Microwave dielectric characterisation of 3D-printed BaTiO3/ABS polymer composites. Sci. Rep. 2016, 6, 22714.

91. Wu, Y.; Isakov, D.; Grant, P.S. Fabrication of Composite Filaments with High Dielectric Permittivity

9 cations Tampa,

9 , B.; on of a

9 DM-3D

9 printing 07147.

9 Polymer-

9 eling 3D printing in pharmaceutical applications. Where are we now? Adv. Drug Deliv. Rev. 2021, 175, 113810.

Compositions	Multi-Material 3D Printing Techniques	Applications	Properties	Ref.
Dielectric material (ink): $Pb_{0.97}La_{0.02}Zr_{0.53}Ti_{0.47}O_3$ + ethylene glycol + ethanolamine Electrode material (ink): Ag	IJP	Capacitors	/	[123]
Dielectric material (ink): $Ba_{0.6}Sr_{0.4}TiO_3$ + Poly (ethylene glycol) diacrylate Electrode material (ink): Ag	IJP	Multilayer ceramic capacitors	The multilayer ceramic capacitors showed a capacitance density of ≈ 500 pF/mm^2	[124]
Dielectric material (ink): $BaO-Al_2O_3-SiO_2-MnO-TiO_2$ Electrode material (ink): Cu	IJP	Multilayer ceramic substrates	The multilayer ceramic substrate showed a shrinkage ratio of ≈15%	[125]
Dielectric material (ink): $BaTiO_3$ Electrode material (/): Cu	AJP + etching + sputtering + plating	Multilayer ceramic substrates	The multilayer ceramic substrate showed a permittivity of ≈ 3000 and a dielectric loss of ≈ 7% at 1 MHz	[126]
Dielectric material (slurry): Al_2O_3 Electrode material (slurry): tungsten	SLA + DIW	Multilayer ceramic substrates	The multilayer ceramic substrates showed a Young modulus E of ≈ 280 ± 11 GPa	[127]
Dielectric material (ink): ZrO_2 Electrode material (ink): Ag	IJP + AJP	Microstrip antennas	The bulk ZrO_2 showed a relative permittivity of 23 and	[128]

110. Choi, J.-W.; Kim, H.-C.; Wicker, R. Multi-material stereolithography. J. Mater. Process. Technol. 2011, 211, 318–328.

Compositions	Multi-Material 3D Printing Techniques	Applications	Properties	Ref.
			a loss tangent of 0.0013 at microwave frequencies	
Dielectric material (ink): SiO_2 + hexanediol diacrylate (HDDA) + alkyl-diphenyl oxide disulfonate Electrode material (ink): Cu	IJP	Microstrip antennas	The resistance was 2.43 × 10^{13} Ω·cm (174.3 µm thick dielectric layer)	[129]
Dielectric material (filament): TiO_2 + cyclo-olefin polymer (COP) Electrode material (slurry): Ag	FDM + DIW	Microstrip antennas	The 30% loaded COP-TiO_2 showed a relative permittivity of 4.56 and a loss tangent of 0.0016 after sintering at 1100 °C	[130]
Dielectric material (filament): $NdTi0_3$ + polydimethylsiloxane (PDMS) Electrode material (slurry): Ag	FDM + DIW	Microstrip antennas	The 25% loaded PDMS-$NdTiO_3$ showed a permittivity of 9.22 and a loss tangent of 0.025 at frequencies up to 17 GHz	[131]
Dielectric material (filament): $MgCaTi0_2$ + PDMS Electrode material (slurry): Ag	FDM + DIW	Microstrip antennas	The 19.6 GHz microstrip antenna showed a return loss of 20 dB along with a 10% bandwidth	[132]

121. Friederich, A., Kohler, C., Nikfalazar, M., Wiens, A., Jakoby, R., Bauer, W., Binder, J.R. Inkjet-Printed Metal-Insulator-Metal Capacitors for Tunable Microwave Applications. Int. J. Appl. Ceram. Technol. 2015, 12, E164–E173.

122. Dossou-Yovo, C.; Mougenot, M.; Beaudrouet, E.; Bessaudou, M.; Bernardin, N.; Charifi, F.; Coquet, C.; Borella, M.; Noguera, R.; Modes, C.; et al. Inkjet Printing Technology: A Novel Bottom-up Approach for Multilayer Ceramic Components and High Definition Printed Electronic Devices. J. Microelectron. Electron. Packag. 2012, 9, 187–198.

123. Matavž, A.; Benčan, A.; Kovač, J.; Chung, C.-C.; Jones, J.L.; Trolier-McKinstry, S.; Malič, B.; Bobnar, V. Additive Manufacturing of Ferroelectric-Oxide Thin-Film Multilayer Devices. ACS Appl.

Mater. Interfaces 2019, 11, 45155–45160.

124. Reinheimer, T.; Azmi, R.; Binder, J.R. Polymerizable Ceramic Ink System for Thin Inkjet-Printed Dielectric Layers. ACS Appl. Mater. Interfaces 2019, 12, 2974–2982.

125. Hirao, T.; Hamada, S. Novel Multi-Material 3-Dimensional Low-Temperature Co-Fired Ceramic Base. IEEE Access 2019, 7, 12959–12963.

126. Imanaka, Y.; Amada, H.; Kumasaka, F.; Takahashi, N.; Yamasaki, T.; Ohfuchi, M.; Kaneta, C. Nanoparticulated Dense and Stress-Free Ceramic Thick Film for Material Integration. Adv. Eng. Mater. 2013, 15, 1129–1135.

127. Raynaud, J.; Pateloup, V.; Bernard, M.; Gourdonnaud, D.; Passerieux, D.; Cros, D.; Madrangeas, V.; Michaud, P.; Chartier, T. Hybridization of additive manufacturing processes to build ceramic/metal parts: Example of HTCC. J. Eur. Ceram. Soc. 2021, 41, 2023–2033.

128. Oh, Y.; Bharambe, V.; Mummareddy, B.; Martin, J.; McKnight, J.; Abraham, M.A.; Walker, J.M.; Rogers, K.; Conner, B.; Cortes, P.; et al. Microwave dielectric properties of zirconia fabricated using NanoParticle Jetting™. Addit. Manuf. 2019, 27, 586–594.

129. Lee, J.-Y.; Choi, C.-S.; Hwang, K.-T.; Han, K.-S.; Kim, J.-H.; Nahm, S.; Kim, B.-S. Optimization of Hybrid Ink Formulation and IPL Sintering Process for Ink-Jet 3D Printing. Nanomaterials 2021, 11, 1295.

130. Castro, J.; Rojas, E.; Ross, A.; Weller, T.; Wang, J. High-k and low-loss thermoplastic composites for Fused Deposition Modeling and their application to 3D-printed Ku-band antennas. In Proceedings of the 2016 IEEE MTT-S International Microwave Symposium (IMS), San Francisco, CA, USA, 22–27 May 2016; pp. 1–4.

131. Castro, J.; Rojas, E.; Weller, T.; Wang, J. High-k and low-loss polymer composites with co-fired Nd and Mg-Ca titanates for 3D RF and microwave printed devices: Fabrication and characterization. In Proceedings of the 2015 IEEE 16th Annual Wireless and Microwave Technology Conference (WAMICON), Cocoa Beach, FL, USA, 13–15 April 2015; pp. 1–5.

132. Castro, J.; Rojas-Nastrucci, E.A.; Ross, A.; Weller, T.M.; Wang, J. Fabrication, Modeling, and Application of Ceramic-Thermoplastic Composites for Fused Deposition Modeling of Microwave Components. IEEE Trans. Microw. Theory Tech. 2017, 65, 2073–2084.